THE JOURNAL OF PHYSICAL CHEMISTRY C

Article

pubs.acs.org/JPCC

Reversible Control of the Orientation of Iodine Molecules inside the $AlPO_4$-11 Crystals

Juanmei Hu, Dingdi Wang, Wenhao Guo, Shengwang Du, and Z. K. Tang*

Department of Physics, Nanoscience and Technology Program, The Hong Kong University of Science and Technology, Clear Water Bay, Kowloon, Hong Kong, China

Supporting Information

ABSTRACT: We demonstrate a technique of reversible controlling the orientation of iodine molecules embedded in elliptical nanochannels of an $AlPO_4$-11 (AEL) crystal. We find that the interactions between iodine and water molecules can significantly affect the iodine molecular orientation inside the nanochannels. In well-hydrated AEL crystals, all the iodine molecules are standing along major axes of the elliptical cross sections of the channels. As decreasing the density of water molecules in the channels, the iodine molecules rotate to lie along the channels. The experimental results obtained from polarized Raman spectroscopy agree well with the results of molecular dynamics simulations. As a result, we can tune the pressure and temperature, which effectively modifies the water molecule density inside the channels, to set the spatial orientation of the iodine molecules over entire crystal. At last, we demonstrate a reversible local operation using a focused laser spot. This technique may be used for engineering molecular orientation in nanostructured devices.

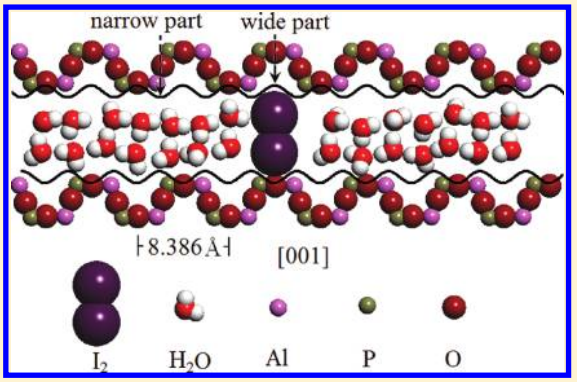

INTRODUCTION

Actively controlling and manipulating the position and orientation of atoms and molecules at nanometer scale is the key for fabricating nanoscale electro-optical devices. Traditionally, atomic and molecular manipulation are obtained using lithographically patterned electromagnetic structures on substrates, such as atom chips,[1−3] single molecule sites,[4,5] and molecular arrays.[6−8] Using scanning probe microscopy is another alternative way to manipulate single atoms and molecules on solid surfaces with a high spatial resolution.[9−11] Recently, with the discovery of many novel nanoporous crystals, intercalating guest atoms and molecules into the matrix of framework materials having pores of molecular dimensions has become a new method to get many interesting nanostructures with extraordinary physical-chemical properties,[12−14] such as the smallest single-wall carbon nanotubes (SWNTs),[15,16] nanoclusters,[17,18] and unidirectional water chains.[19−22] These microporous and nanoporous materials have also been widely used for gas storage[23,24] and separation,[25,26] as well as selective catalytic reactions.[27,28]

Among these nanoporous materials, zeolite single crystals and carbon nanotubes are two widely used materials to adsorb and guide the size matched specimens. For example, isolated helical Se chains were fabricated inside the matrix of $AlPO_4$-5 single crystals by Li et al.[29] Guan et al.[30] succeed to realize La atomic chains inside the carbon nanotubes which is the first dimer chains of rare earth metals. Mann et al.[31] found that one-dimensional protonated water wires in carbon nanotubes have higher affinity than neutral water molecules, which may have applications for charge storage devices. Min et al.[32] obtained uniform directed hemicyanine dyes within channels of silicalite-1 films. Most recently, loading iodine molecules into nanochannels has attracted much research interest due to its possible application in miniature molecular optical clock.[33,34] Guan et al.[35] found that in the confined state the structures of the iodine are SWNTs' diameter dependent, and atomic chains of iodine can only be obtained in critical-sized carbon nanotubes. Fan et al.[36] observed iodine chains with different periodicities inside SWNTs. In addition, depending on the loading of iodine molecules, vaporlike iodine molecules or iodine molecular chains can be formed along the nanochannels of zeolite single crystals.[37,38] It was found that most of these adsorption and reconstruction processes are reversible under certain conditions due to the noncovalent interactions between the adsorbates and the porous materials.

Although zeolites crystals are always hydrophilic, much attention has only been paid to the relationship between the adsorbates and the porous of the materials[39,40] or the properties of the water molecules at different degrees of hydration.[41−43] Little work has been paid to study the effect of the water molecules on the structures and properties of the adsorbates in the nanopores.[44−46]

In this work, the influence of water molecules on the orientation of iodine molecules inside the elliptical nano-

Received: October 31, 2011
Revised: January 15, 2012
Published: January 18, 2012

   dx.doi.org/10.1021/jp210451q | J. Phys. Chem. C 2012, 116, 4423−4430

channels of AEL crystals is systematically studied by means of polarized Raman scattering and molecular dynamics (MD) simulations.[47] The framework of AEL crystal is composed of three types of channels with four, six, and ten rings formed in parallel. Because of the size limitation, the iodine molecules can only be adsorbed in the ten-ring channels with elliptical cross sections. The size of the elliptical channels alternates between wide parts and narrow parts with a period of $c/2$ throughout the channels direction, where c = 8.386 Å is the lattice constant along the channel axis. At the narrow part, the diameters of the major and minor axes of the elliptical channels are only 6.7 and 4.3 Å, respectively, which is comparable to the size of the iodine molecules (see Figure 1). Although it has already been

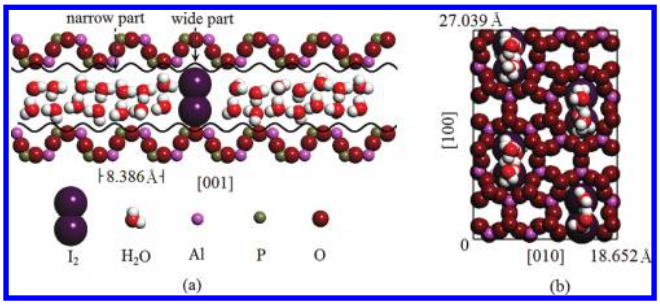

Figure 1. (a) Schematic view of the hydrated AEL channels with low loading iodine molecules. The potential energy described by the quasi-sinusoidal lines at the end of the major axes of the ellipses shows that the channel changes between wide part and narrow part with a period of 1/2 c, where c = 8.386 Å is the lattice constant in the channel axis of the AEL crystal. (b) The low loaded I_2@AEL projected in the (110) plane with periodic conditions.

investigated that the iodine molecules in the elliptical channels of the AEL crystals are restricted in the (101) planes with only two favorite orientations: oriented along the channels direction (lying) and along the major axes of the elliptical cross sections of the channels (standing).[37,38,48] We find that the orientation of the low loading iodine molecules in the AEL crystals (I_2@AEL) can be controlled by different degree of hydration. At saturated hydration, all iodine molecules are oriented along the major axes of the ellipses. When the water molecules are driven out of the channels, the iodine molecules rotate to lie along the channel direction. Moreover, this standing and lying transition is reversible and repeatable due to the physical adsorption of water molecules. MD simulations reproduced the orientation control of the iodine molecules as the experimental observations by different loadings of water molecules. It is the topological match between the AEL channels and the iodine molecules as well as the hydrophilic properties of the AEL crystals that make the single molecular orientation controlled. Three common methods such as environmental pressure, temperature, and laser power have been successfully employed to control the orientation of the iodine molecules in AEL crystals globally and locally, respectively.

EXPERIMENTAL AND COMPUTATIONAL METHODS

Preparation of Hydrated I_2@AEL. The as-synthesized AEL crystals, with a typical dimension of 80 × 40 × 20 μm^3, are first calcined at 680 °C in O_2 atmosphere for 20 h to remove the organic templates of dipropylamine molecules inside the channels and then naturally cooled to room temperature. Before introducing the iodine molecules, the calcined crystals are heated to 100 °C in vacuum condition for 2 h to remove the water molecules. Then the dehydrated empty crystals are sealed together with a small portion of pure iodine source (BDH 99%) in a glass tube at a vacuum of 10^{-2} mbar. With rising temperature, the iodine molecules gradually enter into the channels by physical diffusion. After cooling down to room temperature, the samples are exposed in the air for a few days to remove the excess iodine on the surface of AEL crystals by sublimation. During this process, the water molecules in the air would be naturally absorbed to the AEL channels which are not fully occupied by iodine molecules. In our experiment, the iodine loading is quite low and there are a large amount of water molecules in the channels after hydration equilibrated.

Raman Characterization. The polarized Raman scattering of low loaded I_2@AEL is measured on a micro-Raman system (Jobin Yvon T64000) in backscattering configuration using the 514.5 nm line of Ar-ion laser. The polarizations of the excitation laser and the detection of Raman scattering are in parallel. Linear polarizers are put in the excitation and collection path to strictly control the polarization of the light. During the measurement, the specific polarization on the sample is achieved by rotating the AEL crystals.

MD Simulation Details. The AEL single crystals we used have a space group of *Ima*2 with the lattice constants a = 13.519 Å, b = 18.652 Å, and c = 8.386 Å.[48] The simulation box is set to 2 × 1 × 5 unit cells, which consists of four parallel channels with periodical boundary conditions in all three directions. The schematic view of the hydrated AEL channels with low loading iodine molecules and that projected in the (110) plane are shown in Figure 1. A different loading of water molecules are introduced into the channels which contains only one iodine molecule to mimic the low loading of iodine at different degree of hydration. The loading range of water molecules is from 0 to 30 in each channel of the simulation box.

In the simulations, the Buchart−Universal[49,50] force field is adopted to describe the nonbinding interactions with the charge distribution from ref 51. We describe the AEL framework with Buchart force field and the iodine molecules with Universal force field. The parameters for the AEL−iodine interactions are derived from both force fields with Lorentz−Berthelot combination rules. The van der Waals interactions are modeled in terms of 12−6 Lennard-Jones potentials with a cutoff at 9.2 Å:

$$U_{\text{L-J}}(r_{ij}) = 4\varepsilon_{ij}\left(\left(\frac{\sigma_{ij}}{r_{ij}}\right)^{12} - \left(\frac{\sigma_{ij}}{r_{ij}}\right)^{6}\right) \quad (1)$$

where ε_{ij} is the well depth, σ_{ij} is the collision diameter, and r_{ij} is the distance between the two interacting atoms i and j. The electrostatic interactions are modeled as the Coulomb interactions:

$$U_{\text{Coulomb}}(r_{ij}) = \frac{q_i q_j}{4\pi\varepsilon_0 r_{ij}} \quad (2)$$

where q_i and q_j are the electrostatic charge and r_{ij} is the distance between the two interacting atoms i and j. The long-range Coulomb interactions are calculated by Ewald summation method[52] with a precision of 10^{-4}. The interactions between the water molecules are treated using the SPC/E model.[53] The

dx.doi.org/10.1021/jp210451q | J. Phys. Chem. C 2012, 116, 4423−4430

shake bonds are used for water molecules and the bond stretch of iodine molecules are treated using Morse potential:[54]

$$U(r) = D_e[1 - e^{-\alpha(r-r_e)}]^2 \quad (3)$$

where D_e is the depth of the energy from the bottom of the well to bond dissociation, r_e is the bond length in a given bound state, and α controls the width of the well. The parameters of the nonbond and bond interactions are given in Table 1 and Table 2, respectively.

Table 1. Parameters for Nonbonding Interactions

molecule	atom	ε_i (kcal/mol)	σ_i (Å)	q (e)	m
$AlPO_4$-11	Al	0.0292	3.777	+1.2300	26.9815
	P	0.0629	3.385	+0.3000	30.9737
	O	0.1648	2.940	−0.3825	15.9994
H_2O	O	0.1553	3.166	−0.8476	15.9994
	H	0.0000	0.00	+0.4238	1.0080
iodine	I	0.3390	4.009	0.0000	126.9045

combination rule: $\varepsilon_{ij} = (\varepsilon_{ii} \times \varepsilon_{jj})^{1/2}$ and $\sigma_{ij} = (\sigma_{ii} + \sigma_{jj})/2$

Table 2. Parameters for Bonding Interactions

molecule	bond	bond type	r_e (Å)	D_e (eV)	α (Å^{-1})
iodine	I−I	Morse	2.66	1.544	1.867
water(SPC/E)	H−O	shake	1.00		

All the simulations are carried out in the canonical ensemble (NVT) using LAMMPS[55] package. The velocity−Verlet algorithm with a time step of 0.5 fs is used to integrate the equation of motion. During the simulations, the AEL framework is considered to be fixed and defects free. To ensure the random configurations of the adsorbates, 20 ps annealing is performed from 450 to 300 K in the first stage. Then 4 ns equilibrium runs are performed, followed by 6 ns productive runs for analyzing the statistical properties.

It was reported that the symmetry of the calcined AEL crystal changes from *Ima*2 to *Pna*2 after water adsorption, resulting in a diminished unit-cell volume and more elliptical pores.[56−58] Before systematic simulation, the deformation effect of the AEL crystal on the configuration of the iodine molecules is tested with the atomic coordinates given in ref 58. We find that the deformation of the AEL crystals has little help in making the iodine molecules standing in the channels without the help of the water molecules, though it becomes more elliptical. Therefore, in our simulations the AEL crystal with the symmetry of *Ima*2 is used, and the lattice constant is assumed to be constant and independent of the loading of water molecules.

RESULTS AND DISCUSSION

Figures 2a,b are the sketches of the Raman scattering configurations we used. The incident excitation laser is polarized along the *X*-axis and propagates along the −*Z*-axis. The backscattered signals propagate along the *Z*-axis. The channel direction is denoted as *c*-axis. The intensity of the incident laser on the sample is about 0.8 mW. During the experiments, the polarizations of incident laser and the Raman scattering are in parallel. Thus, the Raman intensity is proportional to the quantity of the iodine molecules along the polarization direction of the laser. As studied before, the iodine molecules in the elliptical channels of AEL crystals are restricted in the (101) plane and have only two perpendicular

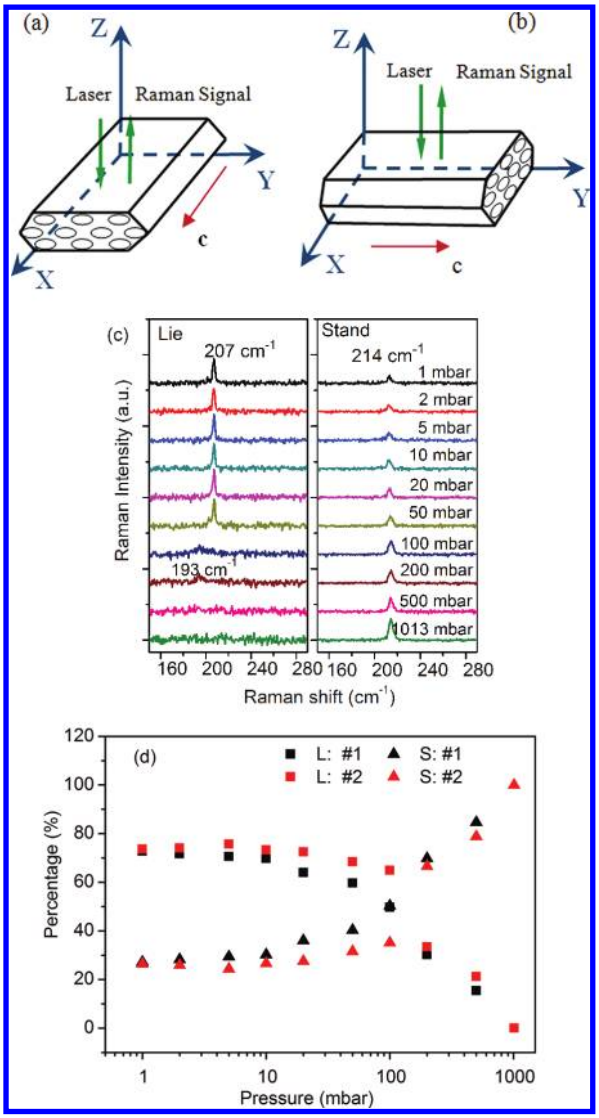

Figure 2. (a, b) Sketches of the Raman scattering configurations. The incident laser is polarized along *X*-axis, and the AEL channels are denoted as the *c*-axes. In (a) the channels of the AEL crystals are parallel to *X*-axis. In (b) the channels of the AEL crystals are parallel to *Y*-axis. (c) Polarized Raman spectra of low loaded I_2@AEL at different pressure with the above two scattering configurations. From bottom to top, the pressure changes from 1013 to 1 mbar. (d) The percentage of lying (denoted by L) and standing (denoted by S) integrated Raman signals of I_2@AEL at different pressure. #1 and #2 are the results of two independent samples.

orientations: either lying along the channel axes or standing along the major axes of the ellipses. Therefore, only the lying iodine molecules can be detected by the Raman scattering with the configuration shown in Figure 2a, while in Figure 2b only the standing iodine molecules can be detected.

The dependence of polarized Raman spectra on environmental pressure taken from the two configurations is shown in Figure 2c. In this experiment, the low loaded I_2@AEL is put in a flat chamber with transparent cover. The chamber is connected to a pump with an adjustable valve and a vacuometer. During Raman scattering, the pressure is fixed to a unique value by controlling the valve. At 1013 mbar, there is only one Raman mode at 214 cm^{-1} which comes from the iodine molecules standing along the major axes of the ellipses,

dx.doi.org/10.1021/jp210451q | J. Phys. Chem. C 2012, 116, 4423−4430

and no Raman signal is detected when the laser is polarized along the channel direction. With decrease of pressure, the intensity of the Raman signal at 214 cm^{-1} decreases monotonously. Meanwhile, a Raman mode at 193 cm^{-1} appears in the lying configuration and its intensity increases. In addition, the lying Raman signals gradually changes from 193 to 207 cm^{-1} when the pressure reaches 50 mbar. The two different Raman shifts of the lying iodine molecules at different pressure come from a different degree of constraint of water molecules. At low vacuum, although part of iodine molecules rotates to lie along the channels, the vicinity of the lying iodine molecules are full of water molecules which will soft the vibration of the iodine molecules and result in a Raman shift at 193 cm^{-1}. When relatively high vacuum is obtained, the water molecules are almost driven out of the channels, and the lying iodine molecules are only constrained by the AEL channel walls, which results in a Raman shift of 207 cm^{-1}. In contrast, the Raman shift of the standing iodine molecules at 214 cm^{-1} is almost not affected by the surrounding water molecules because the water molecules are adsorbed beside the standing iodine molecules instead of adsorbed along the bond direction, as shown in Figure 1a.

The percentage of integrated Raman signals from the two configurations at different environmental pressure is plotted in Figure 2d. The dots marked #1 and #2 in different colors come from two independent samples. The symbols L and S denote the percentage of the iodine molecules with lying and standing configurations, respectively. It clearly shows that under atmospheric pressure all of the iodine molecules have standing configurations. However, the percentage of the standing iodine decreases remarkably with the decrease of the surrounding pressure. At the same time the lying one increases accordingly. This tendency reaches an equilibrium state at about 10 mbar, at which more than 70% of the iodine molecules become lying configurations.

The pressure-dependent orientation of the iodine molecules is related to the variation of the density of water molecules inside the AEL channels at different pressure. The calcined AEL crystal is hydrophilic though it is an electrically neutral material. The partial charged atoms prefer to adsorb polar molecules to balance the local charges. In the low loaded I_2@AEL, most of the channels are empty at the moment the sample are prepared. The moisture in the air will be naturally adsorbed to fully fill the channels and balance the local charges. Thus, under ambient conditions, the iodine molecules are spatially constrained not only by the AEL channels but also by the surrounding water molecules in the channels. The dual confinement makes the iodine molecules have standing configurations in the equilibrium states. With increasing vacuum, the adsorbed water molecules begin to escape from the channels. The iodine molecules in the water-free AEL channels prefer lying along the channels.

To verify the effect of water molecules, we carried out a controlled experiment using dried nitrogen gas (see the Supporting Information). We found that in the dried nitrogen gas the configuration of the iodine molecules inside the AEL crytals remains much like the case in vacuum instead of in ambient air. This result further verifies that it is the polar property of water molecules which makes the iodine molecules standing in channels in thermally equilibrated condition, and the orientation can be controlled by different density of water molecules.

We further explore the underlying mechanism of the orientation of iodine molecules in the hydrated AEL channels with MD simulations from a molecular point of view. Figures 3a and 3b are the snapshots of MD simulations box with 10 and

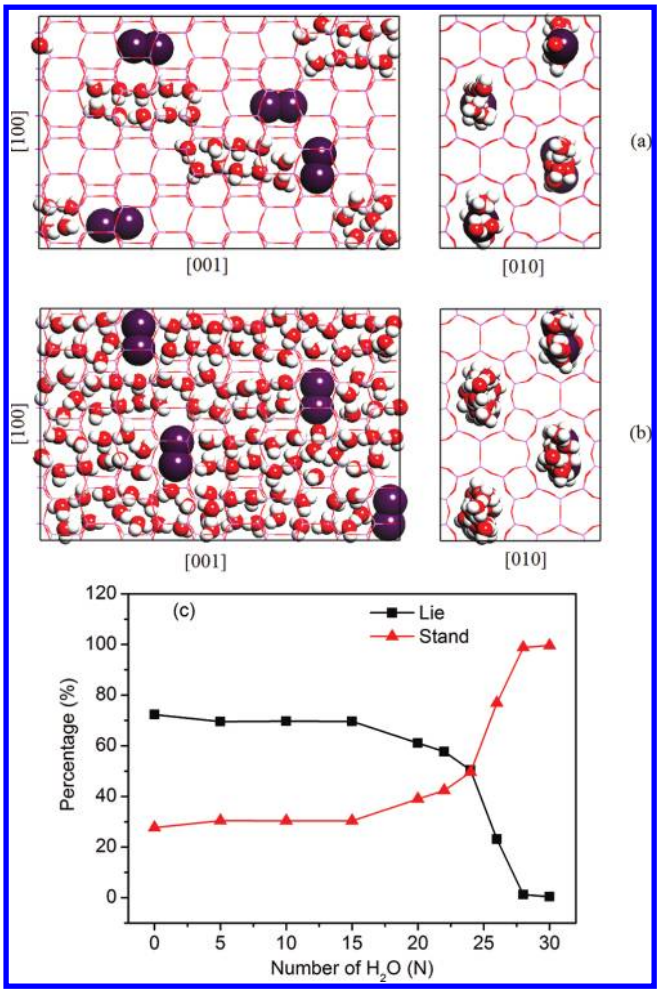

Figure 3. Snapshots of the MD simulations of low loaded I_2@AEL projected in (101) and (110) plane with 10 (a) and 30 (b) water molecules in each channel of simulation box. (c) MD simulation results of the percentage of lying (square) and standing (triangle) iodine molecules as a function of the loading of water molecules.

30 water molecules projected in the (101) and (110) planes, respectively. We can see that at low loading the water molecules like to pack together through hydrogen bonds. The iodine molecules are either separated away from the water molecules or next to the water clusters with one side free. Thus, at low loading of water molecules, the iodine molecules can easily move along the channels. At high loading, the iodine molecules are surrounded by the water molecules, which make the iodine molecules stand up along the major axes of the ellipses with the combination of the framework potential. Figure 3c shows the statistic results of the influence of water molecules on the orientation of iodine molecules. The intensity of the distribution is calculated following the normalized Raman intensity by $I(\theta_i) = [\sum_{n=1}^{N} \cos^4(\theta_n - \theta_i)]/N$, here θ_n is the angle between the projection of the iodine bond in the (101) plane and the channel axis. As has been studied that the iodine molecules are always confined in the (101) plane of AEL crystals, therefore, $\theta_n = 0°$ means the iodine molecule lying

dx.doi.org/10.1021/jp210451q | J. Phys. Chem. C 2012, 116, 4423–4430

along the channel and θ_n = 90° means the standing configuration. The percentage of the standing and lying iodine molecules are calculated by $P_{standing} = I(\theta_{90°})/[I(\theta_{90°}) + I(\theta_{0°})] \times 100\%$ and $P_{lying} = I(\theta_{0°})/[I(\theta_{90°}) + I(\theta_{0°})] \times 100\%$ to follow the experiments results. We can see that at low density of water molecules the iodine molecules in the AEL channels prefer to lie along the channels. The iodine molecules incline to standing up with increasing water molecules. When 30 water molecules are introduced in each channel of the simulation box, all of the iodine molecules are in standing configurations. The MD simulation results are fully consistent with the experimental observations. In addition, during the hydration process, the orientation of the iodine molecules becomes increasingly sensitive to the number of the water molecules, especially near the saturation state.

The potential energy surface of iodine molecules in the AEL channels with different configurations (see in ref 48) tells us that the standing configuration is the most stable state while the lying configuration is a metastable state if only one iodine molecule is considered. These two configurations are interchangeable by overcoming a rotation barrier. In the AEL channels the standing iodine molecules are well restricted due to both the appropriate size of ellipses and their size alternation throughout the channels. The potential energy of the standing iodine increases sharply if it departs from the most stable condition. In contrast, the interactions between the lying iodine molecules and AEL channels are much smoother and the iodine molecules can diffuse forward and backward easily. Because of the thermal motion at room temperature, the iodine molecule tends to have a lying configuration which has lower free energy compared to the well-restricted standing configuration. After hydration, the iodine molecules are surrounded by water molecules. The interactions between water molecules and the AEL crystals are dominated by the Coulomb electrostatic interactions which are much stronger than the van der Waals interactions between iodine molecules and the AEL crystals. Thus, the structures of the adsorbates are the result of a competition between adsorption of water molecules and the orientation selection of iodine molecules. After adsorption saturation, the standing configuration becomes an energetically favorable state against thermal perturbation at 300 K. In that state, the iodine molecules are standing in the wide part of the channels with water molecules blocking at both end of the channel as shown in Figure 1a. Furthermore, the diffusion efficiency of the water molecules is larger than that of the iodine molecules due to the small mass. The water molecules at the end of the channels will escape from the channels easily if the environmental pressure is decreased. Then the water-free iodine molecules in the channels will rotate back to the lying configurations until thermally equilibrated. The detailed analysis shows that the topological match between the AEL channels and iodine molecules as well as the confinement of water molecules are the key roles in the orientation ordering of iodine molecules.

Until now, we have developed an orientation transition mechanism of the confined iodine molecules: the orientation of the iodine molecules confined in AEL crystals is dependent on the loading of water molecules. Because both the iodine molecules and the water molecules are introduced into the channels by physical diffusion, the nonbonding interactions between the adsorbates and the AEL channels can be broken if the thermal motion increases. Thus, temperature effect is used to further test our model.

The temperature dependence of the polarized Raman spectra and the percentage of integrated Raman signals of low loaded I_2@AEL are given in Figure 4. During the measurement, the

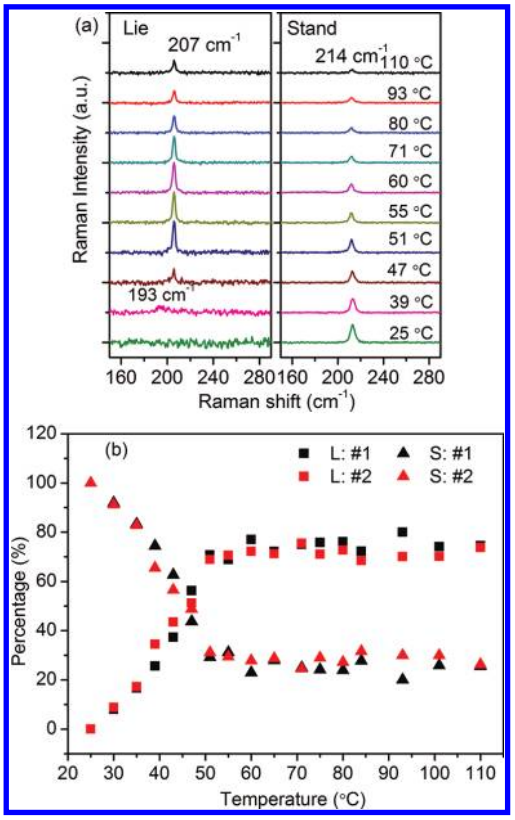

Figure 4. (a) Polarized Raman spectra of the low loaded I_2@AEL measured at different temperature with lying and standing configurations. (b) The percentage of lying (square) and standing (triangle) integrated Raman signals of the I_2@AEL at different temperature. #1 and #2 are the results of two independent samples.

I_2@AEL is put on a heating platform with the crystal directions as shown in Figures 2a,b. The stability of the laser point on the sample is ensured during measurement and the power of incident laser is 1.01 mW. In Figure 4a, we can see that from 25 to 60 °C the standing signal at 214 cm^{-1} decrease while the lying signals at 207 cm^{-1} (193 cm^{-1} at the first stage) increase monotonously from zero, which is quite similar to the dependence of environmental pressure shown in Figure 2c. At a temperature above 60 °C, both the standing and the lying Raman signals decrease because of escaping of the iodine molecules from the channels. Though both signals decrease at high temperature, the percentage of the two signals changes monotonously and become relatively stable even at a temperature above 60 °C, as shown in Figure 4b. The dots marked #1 and #2 in different colors represent the results of two independent samples. We attribute the rapid exchange of the percentage at about 47 °C to the escape of water molecules and the both signals decrease because of desorption of iodine molecules at high temperature.

The two stages desorption of the hydrated I_2@AEL has been confirmed by the thermal gravimetric (TG) curve and the corresponding derivative curve shown in Figure 5. We have to declare that the loading of the iodine used in the TG analysis is much higher than that measured by Raman spectra with the purpose to study the escape temperature of the iodine

dx.doi.org/10.1021/jp210451q | J. Phys. Chem. C 2012, 116, 4423−4430

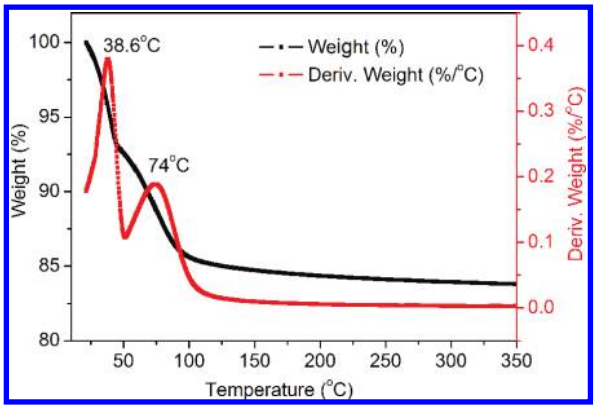

Figure 5. Thermal gravimetric curve and the corresponding derivative curve of high loaded I_2@AEL. The two features of the derivative curve correspond to desorption of water molecules (38.6 °C) and iodine molecules (74 °C).

molecules more clearly. We can see obviously that there are two stages of mass decline with the features at 38.6 and 74 °C, corresponding to desorption of water molecules and iodine molecules, respectively. Thus, with the increase of temperature, the water molecules will be driven out first and left the iodine molecules alone. Simultaneously, the orientation of the confined iodine molecules will transform from standing configurations gradually to lying configurations. The TG analysis of pure hydrated AEL crystals are further used to verify the escape temperature of the water molecules to follow that in low loaded I_2@AEL, as shown in the Supporting Information. The desorption feature of pure hydrated AEL crystals happens at 46 °C instead of 38.6 °C, which is consistent with the temperature at which the percentage of the Raman signals exchange. We have to mention that during the heating process the effect of temperature on the configuration of iodine molecules is negligibly small, and the temperature influence on desorption of water molecules is a dominant factor that determines the configurations of the iodine molecules in hydrated AEL crystals.

Since temperature can be used to control the orientation of the iodine molecules, the heating by laser irradiation may also be feasible as the same effect of temperature. Besides, the laser can locally control the configurations of iodine molecules instead of globally control. Moreover, the water molecules can be reversibly absorbed or desorbed from the AEL channels,[59] which makes the orientation transition of iodine molecules repeatable and reversible.

The power of the incident laser ranges from 1.01 to 10.0 mW and then back to 1.01 mW. The irradiated area is about 4 μm^2. From the polarized Raman spectra in Figure 6a, we can see that with lower incident laser power there is only standing Raman mode at 214 cm^{-1}. As we increase the laser power, the lying signal becomes stronger and the standing signal becomes weaker. This phenomenon is almost the same as temperature effect discussed above. The coappearance of the lying signals of 193 and 207 cm^{-1} at 5.63 mW is the result of Gaussian distribution of the laser power. Clearly, when the power of laser changes back from 10 to 1.01 mW, the lying signals disappear and the intensity of the standing signals increase again, though the intensity is smaller than that of the forward process. The percentage of the integrated lying and standing Raman signals with increasing (black curves) and decreasing (red curves) laser power in Figure 6b shows that the forward and backward

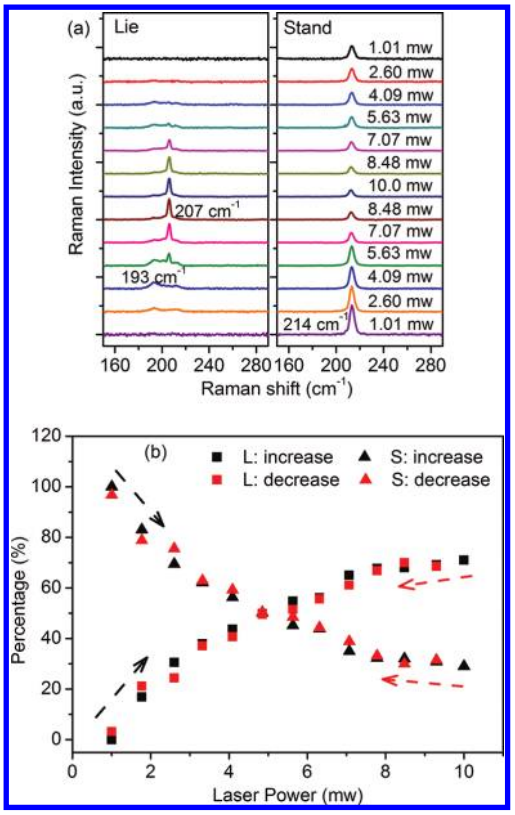

Figure 6. (a) Polarized Raman spectra of low loaded I_2@AEL measured at different laser power with the lying and standing configurations. The laser power increases from 1.01 to 10 mW and then reverses back. (b) The percentage of lying (square) and standing (triangle) integrated Raman signals of the I_2@AEL with increase and decrease of laser power. The arrows represent the sequence of the data in the same color.

percentages coincide quite well. During the laser heating, the water molecules within the laser spot diffuse to the surroundings at a lower temperature, but the iodine molecules still stay there. When the laser power decreases, the surrounding water molecules quickly fill up the interspaces around the iodine molecules. This laser power effect confirms the repeatable and reversible control of iodine molecular orientation by hydrating and dehydrating the AEL crystals. Thus, with the help of laser irradiation, the orientation of the iodine molecules can be switched quickly between these two configurations.

CONCLUSIONS

In summary, the spatial orientation of the neutral iodine molecules inside the nanochannels of AEL crystals is systematically studied by means of polarized Raman scattering and MD simulations. In the AEL crystals, the iodine molecules can self-assemble to a unique and stable direction with the help of water molecules which are naturally adsorbed in the calcined AEL crystals. Moreover, the molecular orientation can be precisely manipulated by controlling the density of the water adsorbed inside the crystal. After removing the water molecules, the iodine molecules change their orientation from the standing configuration to lying along the channels, and thus are rotated by 90°. This phenomenon has been experimentally validated by environmental pressure and temperature. In addition, with the help of laser irradiation, we successfully demonstrated a

dx.doi.org/10.1021/jp210451q | J. Phys. Chem. C 2012, 116, 4423−4430

reversible local control of the orientation of the iodine molecules. From the MD simulations, we find that the size match between AEL channels and the iodine molecules as well as the hydrophilic nature of the AEL crystals play the key roles in this controllable process. The confinement-induced orientation control of the neutral molecules is a novel way of self-assembly. As compared to other mechanical and chemical operations, both physical and chemical properties of the adsorbates are well maintained without any damage in our reversible process. Our result will find applications in engineering nanostructured devices at single molecule level.

■ ASSOCIATED CONTENT

Supporting Information

Coordinates of AEL crystal used in the simulation; polarized Raman spectra of I_2@AEL at different pressure in dried nitrogen gas; thermogravimetric curve of the hydrated AEL crystals without iodine molecules. This material is available free of charge via the Internet at http://pubs.acs.org.

■ AUTHOR INFORMATION

Corresponding Author

*E-mail: phzktang@ust.hk.

Notes

The authors declare no competing financial interest.

■ ACKNOWLEDGMENTS

This research was supported by Hong Kong CERGC Grants 603108 and 604210, HKUST RPC 06/07.SC.06, and Nanoscience and Technology Program at HKUST.

■ REFERENCES

(1) Du, S.; Squires, M. B.; Imai, Y.; Czaia, L.; Saravanan, R. A.; Bright, V.; Reichel, J.; Hänsch, T. W.; Anderson, D. Z. Atom-chip Bose-Einstein Condensation in a Portable Vacuum Cell. *Phys. Rev. A* **2004**, *70*, 053606.

(2) Groth, S.; Krüger, P.; Wildermuth, S.; Folman, R.; Fernholz, T.; Schmiedmayer, J.; Mahalu, D.; Bar-Joseph, I. Atom Chips: Fabrication and Thermal Properties. *Appl. Phys. Lett.* **2004**, *85*, 2980−2982.

(3) Riedel, M. F.; Böhi, P.; Li, Y.; Hänsch, T. W.; Sinatra, A.; Treutlein, P. Atom-Chip-Based Generation of Entanglement for Quantum Metrology. *Nature* **2010**, *464*, 1170−1173.

(4) Nie, S. M.; Emory, S. R. Probing Single Molecules and Single Nanoparticles by Surface-Enhanced Raman Scattering. *Science* **1997**, *275*, 1102−1106.

(5) Selzer, Y.; Cai, L. T.; Cabassi, M. A.; Yao, Y. X.; Tour, J. M.; Mayer, T. S.; Allara, D. L. Effect of Local Environment on Molecular Conduction: Isolated Molecule versus Self-Assembled Monolayer. *Nano Lett.* **2005**, *5*, 61−65.

(6) Aćimović, S. S.; Kreuzer, M. P.; González, M. U.; Quidant, R. Plasmon Near-Field Coupling in Metal Dimers as a Step toward Single-Molecule Sensing. *ACS Nano* **2009**, *3*, 1231−1237.

(7) Fuhrmann, B.; Leipner, H. S.; Höche, H. R.; Schubert, L.; Werner, P.; Gösele, U. Ordered Arrays of Silicon Nanowires Produced by Nanosphere Lithography and Molecular Beam Epitaxy. *Nano Lett.* **2005**, *5*, 2524−2527.

(8) Yan, H.; Park, S. H.; Finkelstein, G.; Reif, J. H.; LaBean, T. H. DNA-Templated Self-Assembly of Protein Arrays and Highly Conductive Nanowires. *Science* **2003**, *301*, 1882−1884.

(9) Ning, Y. S.; Jiang, J.; Shi, Z. L.; Fu, Q.; Liu, J. Z.; Luo, Y.; Tang, B. Z.; Lin, N. Single Molecule's Conductance Depending on Its Orientation. *J. Phys. Chem. C* **2009**, *113*, 26−30.

(10) Wang, S. Y.; Wang, W. H.; Lin, N. Resolving Band-Structure Evolution and Defect-induced States of Single Conjugated Oligomers by Scanning Tunneling Microscopy and Tight-Binding Calculations. *Phys. Rev. Lett.* **2011**, *106*, 206803.

(11) Rief, M.; Oesterhelt, F.; Heymann, B.; Gaub, H. E. Single Molecule Force Spectroscopy on Polysaccharides by Atomic Force Microscopy. *Science* **1997**, *275*, 1295−1297.

(12) Li, L.; Li, G. D.; Yan, C.; Mu, X. Y.; Pan, X. L.; Zou, X. X.; Wang, K. X.; Chen, J. S. Efficient Sunlight-Driven Dehydrogenative Coupling of Methane to Ethane over a Zn^+-Modified Zeolite. *Angew. Chem., Int. Ed.* **2011**, *50*, 8299−8303.

(13) Petkov, V.; Billinge, S. J. L.; Vogt, T.; Ichimura, A. S.; Dye, J. L. Structure of Intercalated Cs in Zeolite ITQ-4: An Array of Metal Ions and Correlated Electrons Confined in a Pseudo-1D Nanoporous Host. *Phys. Rev. Lett.* **2002**, *89*, 075502.

(14) Troche, K. S.; Coluci, V. R.; Braga, S. F.; Chinellato, D. D.; Sato, F.; Legoas, S. B.; Rurali, R.; Galvão, D. S. Prediction of Ordered Phases of Encapsulated C_{60}, C_{70}, and C_{78} Inside Carbon Nanotubes. *Nano Lett.* **2005**, *5*, 349−355.

(15) Wang, N.; Tang, Z. K.; Li, G. D.; Chen, J. S. Single-Walled 4 Å Carbon Nanotube Arrays. *Nature* **2000**, *408*, 50−51.

(16) Lortz, R.; Zhang, Q. C.; Shi, W.; Ye, J. T.; Qiu, C. Y.; Wang, Z.; He, H. T.; Sheng, P.; Qian, T. Z.; Tang, Z. K.; Wang, N.; Zhang, X. X.; Wang, J. N.; Chan, C. T. Superconducting Characteristics of 4-Å Carbon Nanotube-Zeolite Composite. *Proc. Natl. Acad. Sci. U. S. A.* **2009**, *106*, 7299−7303.

(17) Herron, N.; Wang, Y.; Eddy, M. M.; Stucky, G. D.; Cox, D. E.; Moller, K.; Bein, T. Structure and Optical Properties of CdS Superclusters in Zeolite Hosts. *J. Am. Chem. Soc.* **1989**, *111*, 530−540.

(18) Chen, W.; Sammynaiken, R.; Huang, Y. N. Luminescence Enhancement of ZnS: Mn Nanoclusters in Zeolite. *J. Appl. Phys.* **2000**, *88*, 5188−5193.

(19) Hummer, G.; Rasaiah, J. C.; Noworyta, J. P. Water conduction through the hydrophobic channel of a carbon nanotube. *Nature* **2001**, *414*, 188−190.

(20) Su, J. Y.; Guo, H. X. Control of Unidirectional Transport of Single-File Water Molecules through Carbon Nanotubes in an Electric Field. *ACS Nano* **2011**, *5*, 351−359.

(21) Chaban, V. V.; Prezhdo, O. V. Water Boiling Inside Carbon Nanotubes: Toward Efficient Drug Release. *ACS Nano* **2011**, *5*, 5647−5655.

(22) Fang, H. P.; Wan, R. Z.; Gong, X. J.; Lu, H. J.; Li, S. Y. Dynamics of Single-File Water Chains inside Nanoscale Channels: Physics, Biological Significance and Applications. *J. Phys. D: Appl. Phys.* **2008**, *41*, 103002.

(23) Mojet, B. L.; Eckert, J.; Santen, R. A. V.; Albinati, A.; Lechner, R. E. Evidence for Chemisorbed Molecular Hydrogen in Fe-ZSM5 from Inelastic Neutron Scattering. *J. Am. Chem. Soc.* **2001**, *123*, 8147−8148.

(24) Anderson, C. R.; Coker, D. F.; Eckert, J.; Bug, A. L. R. Computational Study of Molecular Hydrogen in Zeolite Na-A. I. Potential Energy Surfaces and Thermodynamic Separation Factors for Ortho and Para Hydrogen. *J. Chem. Phys.* **1999**, *111*, 7599−7613.

(25) Sherry, H. S.; Barrer, R. M.; Peterson, D. L.; Schoenborn, B. P. Separation of Gases by Zeolites. *Science* **1966**, *29*, 555−556.

(26) Lai, Z. P.; Bonilla, G.; Diaz, I.; Nery, J. G.; Sujaoti, K.; Amat, M. A.; Kokkoli, E.; Terasaki, O.; Thompson, R. W.; Tsapatsis, M.; Vlachos, D. G. Microstructural Optimization of a Zeolite Membrane for Organic Vapor Separation. *Science* **2003**, *300*, 456−460.

(27) Frei, H. Selective Hydrocarbon Oxidation in Zeolites. *Science* **2006**, *313*, 309−310.

(28) Corma, A.; Rey, F.; Valencia, S.; Jordá, J. L.; Rius, J. A Zeolite with Interconnected 8-, 10- and 12-Ring Pores and Its Unique Catalytic Selectivity. *Nature Mater.* **2003**, *2*, 493−497.

(29) Li, I. L.; Zhai, J. P.; Launois, P.; Ruan, S. C.; Tang, Z. K. Geometry, Phase Stability, and Electronic Properties of Isolated Selenium Chains Incorporated in a Nanoporous Matrix. *J. Am. Chem. Soc.* **2005**, *127*, 16111−16119.

(30) Guan, L. H.; Suenaga, K.; Okubo, S.; Okazaki, T.; Iijima, S. Metallic Wires of Lanthanum Atoms Inside Carbon Nanotubes. *J. Am. Chem. Soc.* **2008**, *130*, 2162−2163.

(31) Mann, D. J.; Halls, M. D. Water Alignment and Proton Conduction inside Carbon Nanotubes. *Phys. Rev. Lett.* **2003**, *90*, 195503.
(32) Min, H.; Jeon, Y.; Sung, J.; Seok, S.; Kim, D.; Kim, H.; Yoon, K. B. Determination of Absolute Orientations of Hemicyanine Dyes Incorporated into the Channels of Silicalite-1 Films. *J. Phys. Chem. C* **2007**, *111*, 18159−18163.
(33) Guo, W.; Wang, D. D.; Hu, J. M.; Tang, Z. K.; Du, S. Raman Spectroscopy of Iodine Molecules Trapped in Zeolite Crystals. *Appl. Phys. Lett.* **2011**, *98*, 043105.
(34) Ye, J.; Ma, L. S.; Hall, J. L. Molecular Iodine Clock. *Phys. Rev. Lett.* **2001**, *87*, 270801.
(35) Guan, L. H.; Suenaga, K.; Shi, Z. J.; Gu, Z. N.; Lijima, S. Polymorphic Structures of Iodine and Their Phase Transition in Confined Nanospace. *Nano Lett.* **2007**, *7*, 1532−1535.
(36) Fan, X.; Dickey, E. C.; Eklund, P. C.; Williams, K. A.; Grigorian, L.; Buczko, R.; Pantelides, S. T.; Pennycook, S. J. Atomic Arrangement of Iodine Atoms inside Single-Walled Carbon Nanotubes. *Phys. Rev. Lett.* **2000**, *84*, 4621−4624.
(37) Zhai, J. P.; Li, I. L.; Ruan, S. C.; Lee, H. F.; Tang, Z. K. Controlling the Alignment of Neutral Iodine Molecules in the Elliptical Channels of $AlPO_4$-11 Crystals. *Appl. Phys. Lett.* **2008**, *92*, 043117.
(38) Zhai, J. P.; Lee, H. F.; Li, I. L.; Ruan, S. C.; Tang, Z. K. Synthesis and Characterization of Iodine Molecular Wires in Channels of Zeolite AEL Single Crystals. *Nanotechnology* **2008**, *19*, 175604.
(39) Moor, B. A. D.; Reyniers, M. F.; Gobin, O. C.; Lercher, J. A.; Marin, G. B. Adsorption of C2-C8 *n*-Alkanes in Zeolites. *J. Phys. Chem. C* **2011**, *115*, 1204−1219.
(40) Bhide, S. Y.; Yashonath, S. *n*-Pentane and Isopentane in One-Dimensional Channels. *J. Am. Chem. Soc.* **2003**, *125*, 7425−7434.
(41) Demontis, P.; González, J. G.; Jobic, H.; Masia, M.; Sale, R.; Suffritti, G. B. Dynamical Properties of Confined Water Nanoclusters: Simulation Study of Hydrated Zeolite NaA: Structural and Vibrational Properties. *ACS Nano* **2008**, *2*, 1603−1614.
(42) Demontis, P.; González, J. G.; Masia, M.; Suffritti, G. B. The Behaviour of Water Confined in Zeolites: Molecular Dynamics Simulations versus Experiment. *J. Phys.: Condens. Matter* **2010**, *22*, 284106.
(43) Demontis, P.; Stara, G.; Suffritti, G. B. Molecular Dynamics Simulation of Anomalous Diffusion of One-dimensional Water Molecule Chains in Li-ABW Zeolite. *Microporous Mesoporous Mater.* **2005**, *86*, 166−175.
(44) Edery, A. M.; Abdallah, K.; Grenier, P.; Meunier, F. Influence of Traces of Water on Adsorption and Diffusion of Hydrocarbons in NaX Zeolite. *Adsorption* **2001**, *7*, 17−25.
(45) Germanus, A.; Kärger, J.; Pfeifer, H. Self-Diffusion of Paraffins and Olefins in Zeolite NaX Under the Influence of Residual Water Molecules. *Zeolites* **1984**, *4*, 188−190.
(46) Ramamurthy, V.; Sanderson, D. R.; Eaton, D. F. Control of Dye Assembly within Zeolites: Role of Water. *J. Am. Chem. Soc.* **1993**, *115*, 10438−10439.
(47) Catlow, C. R. A.; van Santen, R. A.; Smit, B. *Computer Modelling of Microporous Materials*; Elsevier Academic Press: London, 2004.
(48) Hu, J. M.; Zhai, J. P.; Wu, F. M.; Tang, Z. K. Molecular Dynamics Study of the Structures and Dynamics of the Iodine Molecules Confined in $AlPO_4$-11 Crystals. *J. Phys. Chem. B* **2010**, *114*, 16481−16486.
(49) Burchart, E. D. V.; Bekkum, H. V.; Graaf, B. V. D.; Vogt, E. T. C. A Consistent Molecular Mechanics Force Field for Aluminophosphates. *J. Chem. Soc., Faraday Trans.* **1992**, *88*, 2761−2769.
(50) Rappé, A. K.; Casewit, C. J.; Colwell, K. S.; Goddard, W. A. III; Skiff, W. M. UFF, a Full Periodic Table Force Field for Molecular Mechanics and Molecular Dynamics Simulations. *J. Am. Chem. Soc.* **1992**, *114*, 10024−10035.
(51) Choi, K. J.; Jhon, M. S.; No, K. T. Theoretical Studies on Aluminophosphate-5 ($AlPO_4$-5). *Bull. Korean Chem. Soc.* **1987**, *8*, 155.
(52) Essman, U.; Perera, L.; Berkowitz, M. L.; Darden, T.; Lee, H.; Pedersen, L. G. A Smooth Particle Mesh Ewald Method. *J. Chem. Phys.* **1995**, *103*, 8577−8593.
(53) Berendsen, H. J. C.; Grigera, J. R.; Straatsma, T. P. The Missing Term in Effective Pair Potentialst. *J. Phys. Chem.* **1987**, *91*, 6269−6271.
(54) Morse, P. M. Diatomic Molecules According to the Wave Mechanics, II Vibrational Levels. *Phys. Rev.* **1929**, *34*, 57−64.
(55) Plimpton, S. Fast Parallel Algorithms for Short-Range Molecular Dynamics. *J. Comput. Phys.* **1995**, *117*, 1−19.
(56) Peeters, M. P. J.; Haan, J. W. D.; Ven, L. J. M. V. D.; Hooff, J. H. C. V. Hydration of $AlPO_4$-11 Studied with X-ray Powder Diffraction and ^{27}Al and ^{31}P NMR. *J. Phys. Chem.* **1993**, *97*, 5363−5369.
(57) Tapp, N. J.; Milestone, N. B.; Bowden, M. E.; Meinhold, R. H. Water Adsorption on $AlPO_4$-11: Structural Changes. *Zeolites* **1990**, *10*, 105−110.
(58) Khouzami, R.; Coudurier, G.; Lefebvre, F.; Vedrine, J. C.; Mentzen, B. F. X-ray Diffraction and Solid-State N.M.R. Studies of AEL Molecular Sieves: Effect of Hydration. *Zeolites* **1990**, *10*, 183−188.
(59) Prasad, S.; Balakrishnan, I.; Vetrivel, R. Modeling and MASNMR Spectroscopic Studies on Molecular Sieves. 2. The Nature of Water Molecules in Hydrated $ALPO_4$-11 Host Lattice. *J. Phys. Chem.* **1992**, *96*, 3096−3100.